




# *In Vitro* Insights into the Surface Charge Specificities of Mesoporous Silica Nanoparticles for Bacterial Interactions

Divya Sree H. R. <sup>1</sup>, Gousiya Begum Shaik <sup>1</sup>, Naveenkumar Kontham <sup>2</sup>, Preethi Gurappa gari <sup>1</sup>, Satyanarayana Swamy Vyshnava <sup>1</sup>, Muralidhara Rao Dowlathabad <sup>1,\*</sup>

<sup>1</sup> Department of Biotechnology, University College of Sciences, Sri Krishnadevaraya University, SV Puram, Anantapuramu-515003, Andhra Pradesh, India

<sup>2</sup> Department of Biotechnology, Government Degree College, Anantapuramu-515003, Andhra Pradesh, India

\* Correspondence: rao.muralidharaa@gmail.com;

Scopus Author ID 35265050200

Received: 26.05.2024; Accepted: 6.10.2024; Published: 14.02.2025

**Abstract:** This study demonstrated the influence of mesoporous silica nanoparticles infused with FITC (MSN) and have been changed on the surface with various functional groups (-NH<sub>3</sub>, -COOH, and -PEG) on specific bacterial colonies. The successful doping of FITC was confirmed using UV-Vis spectroscopy, while TEM and SEM investigations verified the homogeneous spherical morphology with an average size of 60.0 ± 2.3 nm. The elemental composition of silicon and oxygen was confirmed using EDX analysis. The application of surface changes led to noticeable differences in both the size and zeta potential. The antibacterial investigations demonstrated that MSNs, changed with -NH<sub>3</sub>, displayed the greatest effectiveness against gram-negative bacteria. On the other hand, -COOH modified fMSNs showed higher efficacy against gram-positive bacteria. PEGylated functionalized MSNs exhibited a moderate level of antimicrobial efficacy against both types of bacteria. The results highlight the importance of surface charge in determining the antibacterial efficacy of MSNs.

**Keywords:** antibacterial agents; bacteria; FITC doping; mesoporous nanoparticles; surface modifications; surface charges.

© 2025 by the authors. This article is an open-access article distributed under the terms and conditions of the Creative Commons Attribution (CC BY) license (<https://creativecommons.org/licenses/by/4.0/>).

## 1. Introduction

Mesoporous silica nanoparticles (MSNs) are widely recognized in the field of nanotechnology for their distinctive physical and chemical properties, which offer substantial advantages in drug delivery and diagnostic applications [1,2]. The surface charge of MSNs is crucial in determining their interactions with biocompatible applications such as the growth of bacterial cells [3]. The significance of this component cannot be overstated when it comes to developing effective antibacterial strategies and acquiring a more profound understanding of the mechanisms underlying bacterial resistance [4]. MSNs particles are recognized for their substantial surface area, versatility in pore diameters, and adaptability for surface modifications to cater to diverse biomedical applications [5].

The surface charges of these nanoparticles can be targeted to manipulate their interactions with bacteria by adjusting the electrostatic interactions between the nanoparticle surface and the bacterial cell walls [6-8]. By modifying MSNs with various functional groups, the interactions with bacterial membranes can be modified, contingent upon the overall surface

charge introduced by the functional groups [9,10]. Many research groups demonstrated that the surface charge of MSNs is a key factor in influencing their capacity to attach to and penetrate bacterial cells [11,12]. Positively charged MSNs exhibit a greater affinity for binding to negatively charged bacterial cell walls [13]. The cell walls of gram-negative bacteria consist of lipopolysaccharides, while gram-positive bacteria have cell walls composed of teichoic acids [14]. The electrostatic attraction between nanoparticles and bacteria boosts the nanoparticles' ability to penetrate the bacterium, impacting the efficacy of drug delivery systems that utilize nanoparticles and the overall antibacterial activity [15].

Modulating the surface charge of MSNs enables careful regulation of the release of antibacterial therapeutics [14]. This property is essential for maintaining the efficacy of treatment over extended durations and minimizing the emergence of bacterial resistance. Furthermore, the composition of MSNs can include surface-bound stimuli-responsive molecules that modify their function in response to environmental cues, such as variations in pH or ionic strength [16]. Furthermore, the surface charge of MSNs makes them exceptionally well-suited for developing antibacterial surfaces, in addition to their use in fluid environments [17]. These specially engineered surfaces can prevent the growth of pathogens and the formation of biofilms on medical devices, reducing the frequency and severity of infections associated with the devices. The effectiveness of these surfaces mostly arises from the favorable interactions between the charged surfaces of MSNs and bacterial membranes, which hinder the usual attachment and growth of bacteria without posing a risk to human cells [18].

Therefore, the comprehensive analysis of the impact of surface charge on the interactions between MSNs and bacterial cells reveals significant findings. These results are essential for advancing our understanding of the interactions between nanoparticles and bacteria and for developing more effective antibacterial treatments and coatings that can combat infection without worsening the problem of antibiotic resistance.

## 2. Materials and Methods

### 2.1. Chemicals and reagents.

In this study, high purity GC-grade chemicals include tetraethyl orthosilicate (TEOS,  $\geq 99.0\%$ ), cetyltrimethylammonium bromide (CTAB, 99.0%), fluorescein isothiocyanate (FITC, 90%), 3-aminopropyltriethoxysilane (APTES, 98%) 3-(aminopropyl)trimethoxysilane (APTMS, 97%), 3-(triethoxysilyl)propyl isocyanate (TESPIC, 95%), poly(ethylene glycol) silane (PEG-silane, 95%) were purchased from SRL chemicals, hydrochloric acid (HCl, 37%), Ammonia solution (28-30%  $\text{NH}_3$ ), and ethanol (99.5%) were purchased from Fisher Scientific. All chemicals were used without further purification, and we stored them according to the supplier's recommendations. Culture media include the Nutrient Broth (NB), De Man, Rogosa, and Sharpe broth (MRS), Agar-Agar, Mueller-Hinton agar (MHA), and Sterile phosphate buffer saline (PBS) were purchased from the HiMedia Laboratories with a purity greater than 98%, ensuring a reliable growth medium for bacterial cultures.

### 2.2. Synthesis of mesoporous silica nanoparticles.

We approached the systemic synthesis of the FITC-doped mesoporous silica nanoparticles (fMSN) using a two-step procedure involving the conjugation of FITC with APTES and subsequent co-condensation with TEOS, based on the earlier reports with slight modifications [16,19]. In the first step, FITC (0.01 mmol, 3.8 mg) was dissolved in 10 mL of

absolute ethanol (AbEtOH) and mixed with APTES (0.1 mmol, 22.9 mg). This solution was stirred at room temperature for 24 hrs in the dark to prevent photobleaching of FITC and form the FITC-APTES conjugate. After conjugation, the solution was directly added to the MSNs synthesis mixture.

In the second step, CTAB (0.9 g, 2.5 mmol) was dissolved in a mixture of 480 mL of deionized water and 20 mL of AbEtOH, followed by adding 3.5 mL of 28-30% NH<sub>3</sub> solution as a base catalyst. This mixture was stirred vigorously at 700 rpm, and TEOS (8.5 mmol, 1.98 g) was added dropwise over 15 min, together with the FITC-APTES conjugate. The reaction mixture was then stirred continuously at 700 rpm for 4 hrs at 40°C, allowing the formation of fMSN. The resulting nanoparticles were collected via centrifugation at 8000 rpm for 10 min and washed thoroughly with AbEtOH three times to remove unreacted precursors. To eliminate CTAB and form mesopores, the nanoparticles were calcined at 550°C for 5 hrs in dry air. After cooling, the nanoparticles were stored in AbEtOH at 4°C until further use.

### *2.3. Preparation for surface modifications.*

Based on the earlier research reports and standard protocols, we modified the fMSN with charges including positive (+ve), negative (-ve), and neutral charges ( $\pm$ ) for biocompatibility studies [20-25]. To develop a positive surface charge on the fMSN, we used APTMS as the major source of the precursor. The 1 g of fMSN were dispersed in 50 mL of anhydrous AbEtOH. We then added APTMS (0.1 mmol, 17.8 mg) to the dispersion and stirred the mixture at 600 rpm for 6 hrs at room temperature. This process allowed the -NH<sub>3</sub> groups from APTMS to covalently bond to the surface of the nanoparticles via silane condensation reactions, creating +ve charged surfaces (fMSN<sup>+ve</sup>). After the reaction, we washed the fMSN<sup>+ve</sup> three times with AbEtOH to remove unbound reagents and dried them under vacuum at room temperature for 6 hours.

For a -ve surface modification, we employed TESPIC, where 1 g of fMSN was suspended in 50 mL of anhydrous toluene and refluxed with TESPIC (0.1 mmol, 21.4 mg) for 12 hrs at 110°C under a nitrogen atmosphere with continuous stirring at 500 rpm. TESPIC underwent hydrolysis and condensation reactions to introduce -COOH groups onto the surface of the nanoparticles (fMSN<sup>-ve</sup>). After cooling to room temperature, the nanoparticles were collected via centrifugation at 7000 rpm for 10 min. They were washed twice with toluene and thrice with AbEtOH to remove unreacted reagents and dried under vacuum at room temperature for 8 hrs.

We performed PEGylation by conjugating PEG-silane to the fMSN to obtain a neutral surface charge. The 1 g of fMSN was dispersed in 50 mL of AbEtOH, and PEG-silane (0.05 mmol, 5.8 mg) was added. The mixture was stirred at 500 rpm for 12 hrs at 50°C to facilitate the attachment of PEG-silane to the fMSN $\pm$ ve. After the reaction, we washed the nanoparticles three times with AbEtOH and dried them under vacuum at room temperature for 6 hrs to ensure neutral charge surfaces. Each set of surfaces modified fMSN was stored in AbEtOH at 4°C until further use.

### *2.4. Characterizations.*

The properties of the synthesized fMSNs were completely understood using several characterization techniques. The optical features of the nanoparticles were investigated using UV-visible spectroscopy, which allowed for the measurement of absorption and fluorescence

emissions (Spectral Max2, Biotek Inc.). The morphology, particle size, and lattice structure were analyzed using transmission electron microscopy (TEM), with the additional recording of selected area electron diffraction (SAED) patterns (TALOS F200S G2). The X-ray diffraction (XRD) spectrum (PANalytical, X-pert PRO) further confirmed the lattice structure. The technique of scanning electron microscopy (SEM) was employed to acquire highly detailed images of particle size. At the same time, energy-dispersive X-ray spectroscopy (EDS) was utilized to analyze and determine the elemental composition of the MSNs (TESCAN and Bruker). FTIR spectroscopy was conducted to determine the functional groups contained in the nanoparticles (Perkin Elmer, Spectrum 1000). The hydrodynamic diameter of the nanoparticles was analyzed using dynamic light scattering (DLS), while the surface charge of the nanoparticles was determined by zeta potential studies (Malvern Nano ZS). The integration of these methods yielded a thorough examination of the structural, optical, and surface characteristics of the synthesized MSNs.

### 2.5. Bacterial cultures.

The bacterial strains *Lactobacillus acidophilus* (MTCC 1408) and *Pseudomonas aeruginosa* (MTCC 7925) were obtained from the Microbial Type Culture Collection (MTCC), Chandigarh, India. The bacterial strains were cultivated in sterile nutrient slants at 37°C to ensure viability and purity. Each slant contained an NA medium specifically formulated to promote optimal growth. To recover and optimize the bacterial cultures, we inoculated each slant with its respective strain and incubated it at 37°C for 48 hrs. After visible growth was observed, single colonies were streaked onto nutrient agar petri plates using the streak plate method. These streak plates were then incubated under the same conditions until isolated colonies developed. For long-term storage, we transferred several single colonies from each streak plate into freshly prepared slants and stored them at 4°C. These slants served as the master cultures for subsequent research experiments. Additionally, for experimental use, we isolated single colonies from the streak plates and cultured them in sterile nutrient broth to ensure the growth of homogenous bacterial populations. The broth cultures were incubated at 37°C and shaken at 100 rpm to achieve a cell density suitable for subsequent biocompatibility studies.

### 2.6. Antimicrobial activity and biocompatibility studies.

We evaluated the biocompatibility of +ve (-NH<sub>3</sub>), -ve (-COOH), and ±ve (-PEG) charged fMSN with *L. acidophilus* and *P. aeruginosa* bacterial strains using the turbidimetric method. The pure cultures of *L. acidophilus* and *P. aeruginosa* prepared bacterial suspensions at a concentration of 1x10<sup>6</sup> colony-forming units per mL (CFU/mL). To conduct the study, we prepared a stock solution of each surface-modified nanoparticle (positive, negative, and neutral) in sterile 1x PBS. From this, we prepared serial dilutions to achieve final concentrations of 0.1, 1.0, 10, 40, 80, 100, 160, and 200 µg/mL.

The bacterial suspensions were aliquoted into sterile 96-well microplates, each containing 100 µL of bacterial suspension. Each surface-modified nanoparticle solution (100 µL) was added to the wells to achieve the final desired concentrations. The wells were then covered and incubated at 37°C with gentle shaking at 100 rpm. We conducted the initial turbidimetric measurements after 12 hrs by measuring the optical density (OD) at 600 nm with a microplate reader (µQuant™, Bio-Teck instruments, USA). Further readings were taken at

24, 48, and 72-hrs intervals to evaluate growth over time. Each condition was tested in triplicate.

The minimum inhibitory concentration (MIC) for each nanoparticle type was calculated as the lowest concentration at which no visible bacterial growth was detected compared to the untreated control. We compared the OD values of each treatment group with the control wells to determine the concentration that inhibited bacterial growth by at least 90%. MIC values were determined for each surface modification type and bacterial strain. We analyzed the data by plotting bacterial growth (OD values) against nanoparticle concentration to determine dose-response curves. Statistical analyses were conducted to identify significant differences in bacterial growth among the different surface-modified nanoparticle types.

### 3. Results and Discussion

In this study, we demonstrated the impact of the impact MSN doped with FITC ( $\mu$ MSN) and have undergone surface modification using different functional groups (-NH<sub>3</sub>, -COOH, and -PEG) on selective bacterial colonies. We successfully synthesized the  $\mu$ MSN, and it was primarily confirmed by using UV-Vis spectroscopy. The characteristic FITC spectral peak was evident in the 430-480 nm range, validating successful doping, as shown in Figure 1a. This observation aligned with the literature, where FITC-doped silica nanoparticles exhibited UV-Vis absorption peaks between 430-490 nm due to the green emission fluorescence properties of FITC [26,27]. TEM images confirmed the porous structure of the  $\mu$ MSN, with an average pore size ranging from 8.0±2.4 nm and a nanoparticle diameter between 60.0±3.0 nm, as shown in Figure 1b. The sizes were consistent with previous studies reporting MSNs diameters within the observed range, which aligns with the expectations of MSNs synthesized through similar sol-gel methods [28]. The SAED pattern showed no distinguishable crystalline structures, indicating an amorphous form for the nanoparticles. The X-ray diffraction (XRD) analysis further confirmed this finding, where no sharp intensity peaks were observed, as shown in Figure 1c. The results are consistent with existing research, where  $\mu$ MSN typically exhibit an amorphous form due to their synthesis conditions [29].

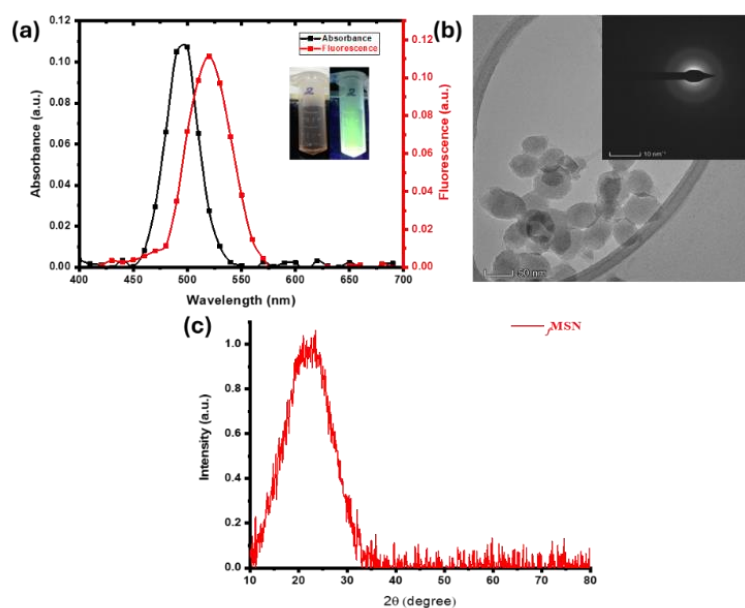


**Figure 1.** (a) UV-visible absorbance and fluorescence spectrum where insight shows the green fluorescence of FITC; (b) Transmission electron microscopic images of the  $\mu$ MSN and insights shows the SEAD pattern of amorphous nature; (c) X-ray diffraction of the amorphous nature of the particles.

Upon analyzing the SEM results, we found that the size of the  $\beta$ MSN results is consistent with the measurements obtained from TEM. The average size was determined to be  $60.0 \pm 2.3$  nm. The  $\beta$ MSN exhibited a high degree of uniformity and possessed a spherical morphology, as shown in Figure 2a. This consistency in particle size and shape is crucial for applications that require uniform particle behavior and interactions [30,31]. The elemental composition of  $\beta$ MSN was validated by analyzing the EDS spectra. The EDS examination detected the existence of silicon (Si) and oxygen (O), which are the main components of silica ( $\text{SiO}_2$ ). The EDX analysis yielded quantitative findings showing that the weight percentages of silicon and oxygen were 61.01% and 38.99%, respectively, as shown in Figure 2b. The error margins for these measurements fell below acceptable thresholds, with a deviation of 3.01% for silicon and 5.94% for oxygen, respectively, aligning with mesoporous silica's anticipated makeup [32,33].

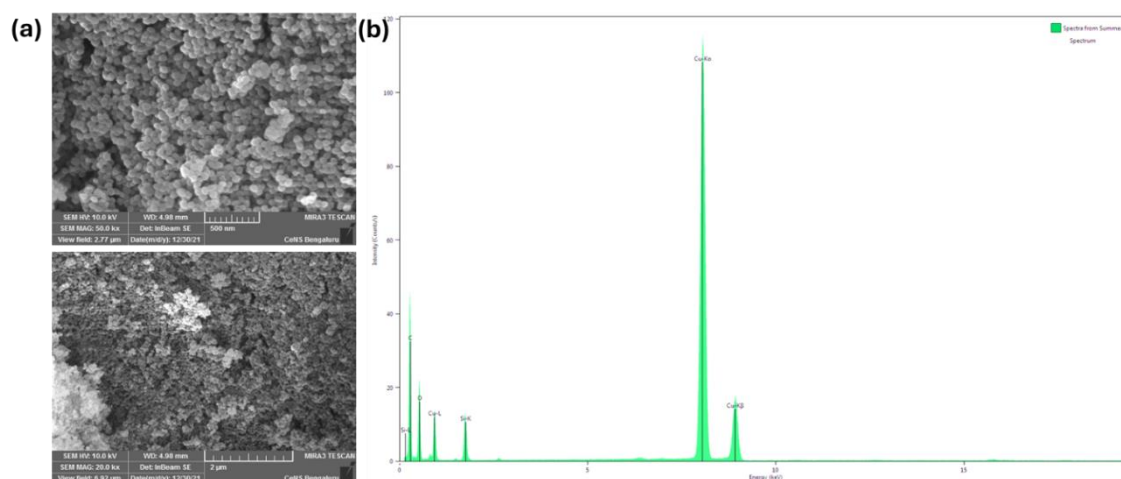


**Figure 2.** (a) Scanning electron microscopic images show the spherical shape of the nanoparticles and uniform size; (b) Electron diffraction spectrum of the nanoparticles shows the elemental compositions.

The surface modifications on the  $\beta$ MSNs were confirmed by various methods, where distinct variations in hydrodynamic size were observed among the various surface changes, as indicated by DLS tests. When compared, the  $\beta$ MSN, which were not subjected to any surface alteration, had an average size of  $60 \pm 2.8$  nm, consistent with the TEM and SEM results. After being treated with  $-\text{NH}_3$ , a small increase in size was detected, with the average size changing to around  $62 \pm 3.3$  nm. In contrast, introducing  $-\text{COOH}$  led to a minor reduction in size, resulting in an average of  $58 \pm 1.9$  nm. The nanoparticles treated with PEG retained a size distribution comparable to that of the unaltered  $\beta$ MSNs, approximately  $60 \pm 3.9$  nm, as shown in Figure 3a. According to the Rizzi research group, modifying the surface of  $\beta$ MSN has a notable impact on their size and stability in water-based solutions. This supports our findings that modification of the surface of nanoparticles results in changes to their size distributions [34]. Similarly, the zeta potential measurements exhibited significant variability depending on the modifications made to the surface. The nanoparticles treated with  $-\text{NH}_3$  showed a significantly high positive zeta potential, with an average value of approximately +30 mV.

On the other hand, nanoparticles that were treated with  $-\text{COOH}$  showed a significantly high negative zeta potential, with an average value of approximately -40 mV. The nanoparticles treated with PEG exhibited a zeta potential close to neutral, approximately -5 mV, suggesting a surface that is generally unreactive and reduces non-specific interactions, as shown in Figure 3b. The respective active peaks for the same particles are observed to confirm the successful modifications of the charged functional groups.

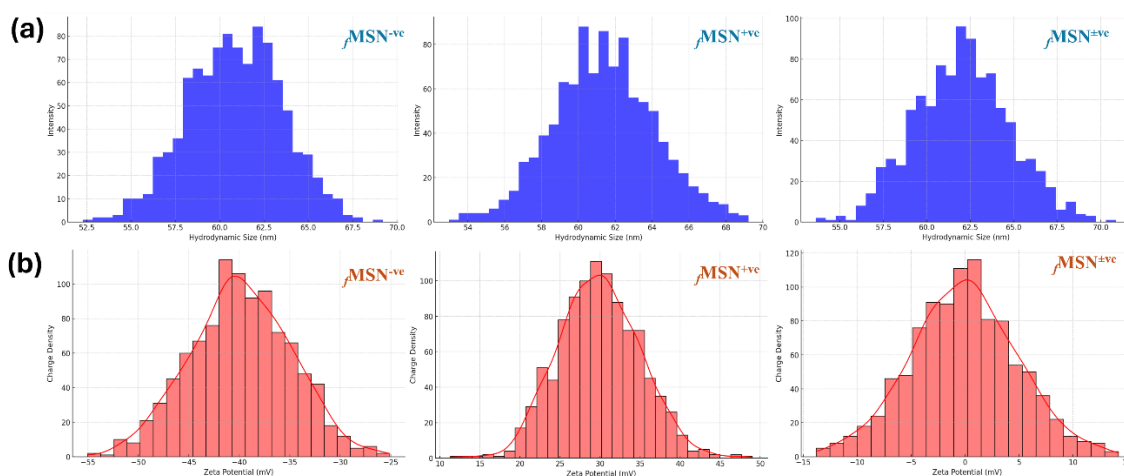


**Figure 3.** (a) Hydrodynamic size of the modified nanoparticles with various surface ligands; (b) Charge distribution of the modified nanoparticles with various surface ligands.

The FTIR spectra validate the effective functionalization of  $f\text{MSN}^{-ve}$ ,  $f\text{MSN}^{+ve}$ , and  $f\text{MSN}^{\pm ve}$ . All samples exhibit a broad peak at approximately  $3498\text{ cm}^{-1}$ , signifying the presence of hydroxyl groups or adsorbed water, alongside consistent Si-O-Si peaks at approximately  $1224\text{ cm}^{-1}$  and  $716\text{ cm}^{-1}$ , affirming the silica framework. The peak at  $1710\text{ cm}^{-1}$  in  $f\text{MSN}^{-ve}$  indicates the presence of carbonyl (C=O) groups, signifying negatively charged functions such as carboxyl groups. In  $f\text{MSN}^{+ve}$ , the C=O peak changes to  $1776\text{ cm}^{-1}$ , presumably due to protonation or amine groups, whilst Si-O-Si vibrations exhibit a small shift. In  $f\text{MSN}^{\pm ve}$ , a novel peak at  $2662\text{ cm}^{-1}$  signifies C-H stretching, demonstrating a balance of positively and negatively charged functions, as shown in Figure 4.

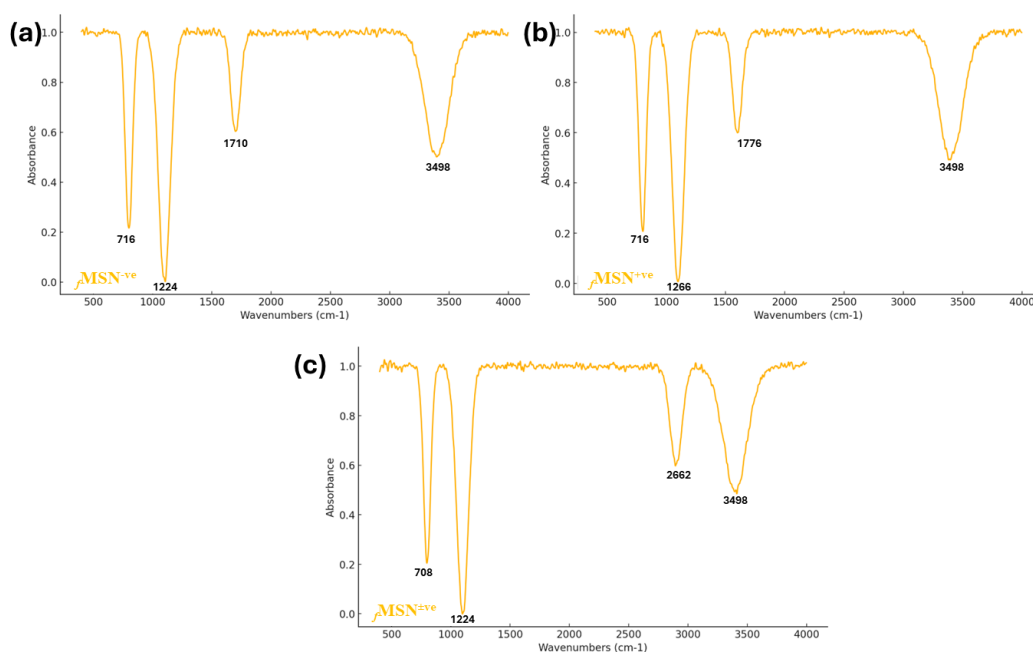


**Figure 4.** FTIR spectral data for the (a)  $f\text{MSN}^{-ve}$ ; (b)  $f\text{MSN}^{+ve}$ ; (c)  $f\text{MSN}^{\pm ve}$ .

We conducted additional studies to examine the antibacterial effectiveness of these  $f\text{MSNs}$  against both *L. acidophilus* and *P. aeruginosa* bacteria. We evaluated bacterial growth in the presence of varying concentrations of  $f\text{MSNs}$  using turbidimetric methods over varied incubation periods (12, 24, 48, and 72 hrs). The relationship between  $f\text{MSNs}$  concentrations and bacterial growth was evident: higher concentrations of  $f\text{MSNs}$  resulted in a substantial

decrease in bacterial growth. The  $-NH_3$ -modified  $fMSN^{+ve}$  exhibited the most potent suppression against gram-negative bacteria, achieving almost 100% inhibition at higher concentrations (160 and 200  $\mu\text{g/mL}$ ) after 72 hrs of incubation. The impact on *L. acidophilus* bacteria was not as strong, suggesting a specific antibacterial effect that is probably caused by the stronger attraction between positively charged  $-NH_3$  groups and the negatively charged outer membrane of gram-negative bacteria. Alavi *et al.* reported that PEGylated liposomes exhibited similar interactions, in which positively charged nanoparticles displayed increased antibacterial activity due to more robust electrostatic contacts [12].

$fMSN^{-ve}$  with COOH exhibited enhanced efficacy against *L. acidophilus* bacteria, resulting in substantial suppression of growth at lower concentrations (80 to 120  $\mu\text{g/mL}$ ) during a 48-hour timeframe. This outcome is consistent with the discoveries made by Abbaszadegan *et al.*, who observed that nanoparticles with a -ve charge exhibited increased interactions with the +vely charged areas of the cell walls in *L. acidophilus* bacteria [35]. The zeta potential data indicates higher connections between -very charged  $-COOH$  groups and positively charged sections of gram-positive bacterial cell walls, supporting this conclusion. PEG-modified  $fMSN^{\pm ve}$  exhibited modest antibacterial activity against both *P. aeruginosa* and *L. acidophilus* bacteria, as shown in Figure 5. However, significant inhibition was only found at higher concentrations (160 and 200  $\mu\text{g/mL}$ ) and longer incubation times. This moderate activity aligns with the neutral zeta potential, suggesting reduced electrostatic interactions. The findings of Rodrigues *et al.* support this view, as they discovered that PEGylated nanoparticles displayed a modest level of antibacterial activity due to their decreased non-specific interactions with bacterial cells [36].

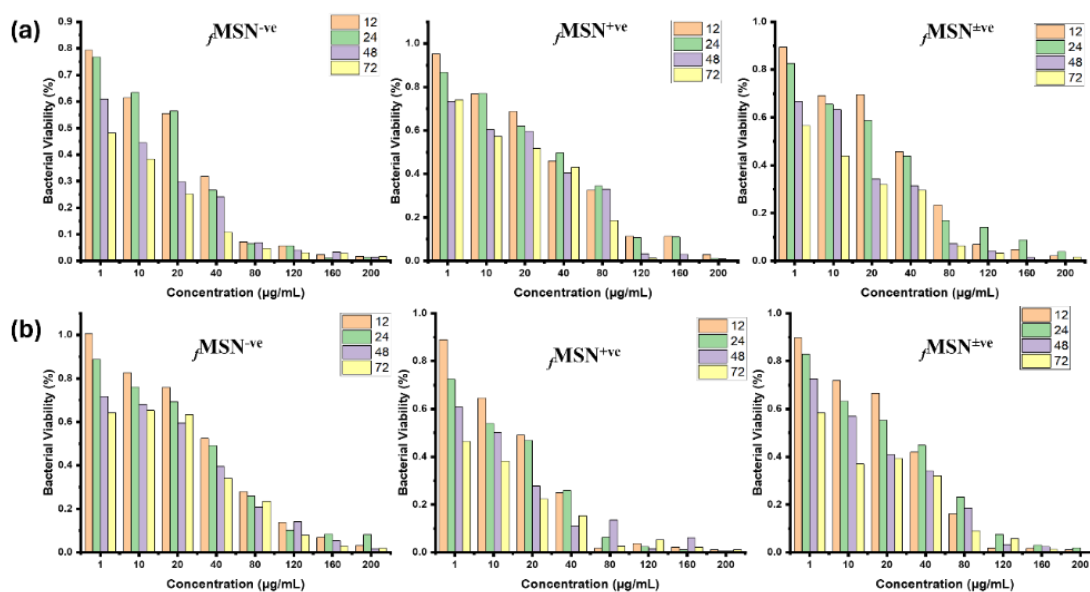


**Figure 5.** Bacterial viability studies with turbidometry (a) *Lactobacillus acidophilus*; (b) *Pseudomonas aeruginosa*.

To measure the effectiveness of the antibacterial properties, we determined the MIC values for each type of  $fMSN$ . The MIC of  $fMSN^{+ve}$  against *P. aeruginosa* bacteria was found to be 40  $\mu\text{g/mL}$  after 24 hrs, which decreased to 20  $\mu\text{g/mL}$  after 72 hrs. The minimum MIC for *L. acidophilus* bacteria was around 80  $\mu\text{g/mL}$  after 72 hrs.  $fMSN^{-ve}$  exhibited a MIC of 40  $\mu\text{g/mL}$  against *L. acidophilus* bacteria after 24 hrs, which decreased to 20  $\mu\text{g/mL}$  after 72 hrs. In contrast, the MIC for *P. aeruginosa* bacteria was 80  $\mu\text{g/mL}$  after 72 hrs. The  $fMSN^{\pm ve}$  exhibited comparable MIC values against both bacterial strains, around 120  $\mu\text{g/mL}$  after 48

hrs, with a small decrease to 80  $\mu\text{g/mL}$  after 72 hrs, as shown in Figure 5. The findings highlight the significance of surface charge in determining the antibacterial effectiveness of nanoparticles. The MIC values obtained in this work align with the findings of Osman *et al.*, who observed that nanoparticles with surface modifications had decreased MIC values as a result of improved interactions with bacterial cells [37].

In addition, we further conducted biocompatibility to assess the possible influence of various incubation times on bacterial proliferation in the presence of these  $\mu\text{MSN}$ . The findings demonstrated that increasing the duration of exposure boosts the antibacterial impact, especially for nanoparticles that have been modified with  $-\text{NH}_3$  and  $-\text{COOH}$ . The  $\mu\text{MSN}$  exhibit a time-dependent enhancement in effectiveness, indicating that they not only hinder bacterial growth but also potentially interfere with cellular activities over extended durations, resulting in increased bacterial mortality. Chen *et al.* conducted a study that supports these results. They found that when bacteria were exposed to nanoparticles for a lengthy period, it led to a greater reduction of growth [38].

#### 4. Conclusions

This study effectively produced and analyzed  $\mu\text{MSN}$  with different surface modifications. The nanoparticles' structural integrity and homogeneity were verified by UV-Vis spectroscopy, TEM, SEM, and EDX studies. The hydrodynamic size and zeta potential of the  $\mu\text{MSN}$  were considerably affected by surface changes. The antibacterial experiments revealed that the surface charge of nanoparticles is a critical factor in determining their effectiveness. The  $\mu\text{MSN}$  changed with  $-\text{NH}_3$  showed the most potent antibacterial action against gram-negative bacteria, whereas the  $\mu\text{MSNs}$  modified with  $-\text{COOH}$  were more efficacious against gram-positive bacteria. PEG-modified  $\mu\text{MSN}$  exhibited moderate antibacterial efficacy against both types of bacteria. The findings offer useful insights for developing efficient antibacterial drugs using nanoparticle technology by employing selective surface changes.

#### Funding

This research received no external funding.

#### Acknowledgments

The authors sincerely acknowledge Sri Krishnadevaraya University's support through laboratory and advanced instrumentation in this research.

#### Conflicts of Interest

The authors declare no conflict of interest.

#### References

1. Manzano, M.; Vallet-Regí, M. Mesoporous silica nanoparticles for drug delivery. *Advanced functional materials* **2020**, *30*, 1902634, <https://doi.org/10.1002/adfm.201902634>.
2. Pu, X.; Li, J.; Qiao, P.; Li, M.; Wang, H.; Zong, L.; Yuan, Q.; Duan, S. Mesoporous silica nanoparticles as a prospective and promising approach for drug delivery and biomedical applications. *Current cancer drug targets* **2019**, *19*, 285-295, <https://doi.org/10.2174/1568009619666181206114904>.

3. Gounani, Z.; Asadollahi, M.A.; Pedersen, J.N.; Lyngsø, J.; Pedersen, J.S.; Arpanaei, A.; Meyer, R.L. Mesoporous silica nanoparticles carrying multiple antibiotics provide enhanced synergistic effect and improved biocompatibility. *Colloids and Surfaces B: Biointerfaces* **2019**, *175*, 498-508, <https://doi.org/10.1016/j.colsurfb.2018.12.035>.
4. Sivamaruthi, B.S.; Thangaleela, S.; Kesika, P.; Suganthy, N.; Chaiyasut, C. Mesoporous silica-based nanoplatforms are theranostic agents for the treatment of inflammatory disorders. *Pharmaceutics* **2023**, *15*, 439, <https://doi.org/10.3390/pharmaceutics15020439>.
5. Tiwari, P.; Yadav, K.; Shukla, R.P.; Gautam, S.; Marwaha, D.; Sharma, M.; Mishra, P.R. Surface modification strategies in translocating nano-vesicles across different barriers and the role of bio-vesicles in improving anticancer therapy. *Journal of Controlled Release* **2023**, *363*, 290-348, <https://doi.org/10.1016/j.jconrel.2023.09.016>.
6. Ladaycia, A.; Passirani, C.; Lepeltier, E. Microbiota and nanoparticles: Description and interactions. *European Journal of Pharmaceutics and Biopharmaceutics* **2021**, *169*, 220-240, <https://doi.org/10.1016/j.ejpb.2021.10.015>.
7. Zhao, H.; Wang, Y.; Bao, L.; Chen, C. Engineering nano-bio interfaces from nanomaterials to nanomedicines. *Accounts of Materials Research* **2022**, *3*, 812-829, <https://doi.org/10.1021/accountsmr.2c00072>.
8. Vitale, S.; Rampazzo, E.; Hiebner, D.; Devlin, H.; Quinn, L.; Prodi, L.; Casey, E. Interaction between engineered pluronic silica nanoparticles and bacterial biofilms: Elucidating the role of nanoparticle surface chemistry and EPS matrix. *ACS Applied Materials & Interfaces* **2022**, *14*, 34502-34512, <https://doi.org/10.1021/acsami.2c10347>.
9. Yusuf, A.; Almotairy, A.R.Z.; Henidi, H.; Alshehri, O.Y.; Aldughaim, M.S. Nanoparticles as Drug Delivery Systems: A Review of the implication of nanoparticles' physicochemical properties on responses in biological systems. *Polymers* **2023**, *15*, 1596, <https://doi.org/10.3390/polym15071596>.
10. Mahanta, U.; Khandelwal, M.; Deshpande, A.S. Antimicrobial surfaces: a review of synthetic approaches, applicability and outlook. *Journal of Materials Science* **2021**, *56*, 17915-17941, <https://doi.org/10.1007/s10853-021-06404-0>.
11. Aguilar-Colomer, A.; Colilla, M.; Izquierdo-Barba, I.; Jimenez-Jimenez, C.; Mahillo, I.; Esteban, J.; Vallet-Regí, M. Impact of the antibiotic-cargo from MSNs on gram-positive and gram-negative bacterial biofilms. *Microporous and Mesoporous Materials* **2021**, *311*, 110681, <https://doi.org/10.1016/j.micromeso.2020.110681>.
12. Alavi, M.; Thomas, S.; Sreedharan, M. Modification of silica nanoparticles for antibacterial activities: mechanism of action. *Micro Nano Bio Aspects* **2022**, *1*, 49-58, <https://doi.org/10.22034/MNBA.2022.153448>.
13. Zhuang, J.; Yu, Y.; Lu, R. Mesoporous silica nanoparticles as carrier to overcome bacterial drug resistant barriers. *International Journal of Pharmaceutics* **2023**, *631*, 122529, <https://doi.org/10.1016/j.ijpharm.2022.122529>.
14. Colilla, M.; Vallet-Regí, M. Organically Modified Mesoporous Silica Nanoparticles against Bacterial Resistance. *Chemistry of Materials* **2023**, *35*, 8788-8805, <https://doi.org/10.1021/acs.chemmater.3c02192>.
15. Álvarez, E.; González, B.; Lozano, D.; Doadrio, A.L.; Colilla, M.; Izquierdo-Barba, I. Nanoantibiotics Based in Mesoporous Silica Nanoparticles: New Formulations for Bacterial Infection Treatment. *Pharmaceutics* **2021**, *13*, 2033, <https://doi.org/10.3390/pharmaceutics13122033>.
16. Zhou, S.; Zhong, Q.; Wang, Y.; Hu, P.; Zhong, W.; Huang, C.-B.; Yu, Z.-Q.; Ding, C.-D.; Liu, H.; Fu, J. Chemically engineered mesoporous silica nanoparticles-based intelligent delivery systems for theranostic applications in multiple cancerous/non-cancerous diseases. *Coordination Chemistry Reviews* **2022**, *452*, 214309, <https://doi.org/10.1016/j.ccr.2021.214309>.
17. Patel, U.S. Nanomaterials in theranostics: therapeutics and diagnosis against infectious diseases. Dissertation Thesis, The University of Alabama in Huntsville, **2022**.
18. Liu, Y.; Wu, Y.; Luo, Z.; Li, M. Designing supramolecular self-assembly nanomaterials as stimuli-responsive drug delivery platforms for cancer therapy. *Iscience* **2023**, *26*, 106279, <https://doi.org/10.1016/j.isci.2023.106279>.
19. Li, Z. Synthesis and Derivatization of Stimuli Responsive Mesoporous Silica Nanoparticles and Biomedical Drug Delivery Application. Doctor Thesis, University of California, Los Angeles, **2015**.

20. Erkan, H.; Keçeciler-emir, C.; Özel, C.; Yücel, S. Posaconazole loading and release behavior in surface-modified mesoporous silica nanoparticulate system. *Erzincan University Journal of Science and Technology* **2023**, *16*, 615-632, <https://doi.org/10.18185/erzifbed.1189339>.
21. Dadej, A.; Woźniak-Braszak, A.; Bilski, P.; Piotrowska-Kempisty, H.; Józkowiak, M.; Stawny, M.; Dadej, D.; Mrotek, M.; Jelińska, A. APTES-Modified SBA-15 as a non-toxic carrier for phenylbutazone. *Materials* **2022**, *15*, 946, <https://doi.org/10.3390/ma15030946>.
22. Flores, D.; Almeida, C.M.R.; Gomes, C.R.; Balula, S.S.; Granadeiro, C.M. Tailoring of mesoporous silica-based materials for enhanced water pollutants removal. *Molecules* **2023**, *28*, 4038, <https://doi.org/10.3390/molecules28104038>.
23. Beitzinger, B.; Gerbl, F.; Vomhof, T.; Schmid, R.; Noschka, R.; Rodriguez, A.; Wiese, S.; Weidinger, G.; Ständker, L.; Walther, P. Delivery by Dendritic Mesoporous Silica Nanoparticles Enhances the Antimicrobial Activity of a Napsin-Derived Peptide Against Intracellular Mycobacterium tuberculosis. *Advanced healthcare materials* **2021**, *10*, 2100453, <https://doi.org/10.1002/adhm.202100453>.
24. von Baeckmann, C.; Kählig, H.; Lindén, M.; Kleitz, F. On the importance of the linking chemistry for the PEGylation of mesoporous silica nanoparticles. *Journal of Colloid and Interface Science* **2021**, *589*, 453-461, <https://doi.org/10.1016/j.jcis.2020.12.004>.
25. Siddiqui, B.; Haq, I.-u.; Al-Dossary, A.A.; Elaissari, A.; Ahmed, N. Exploiting recent trends for the synthesis and surface functionalization of mesoporous silica nanoparticles towards biomedical applications. *International Journal of Pharmaceutics: X* **2022**, *4*, 100116, <https://doi.org/10.1016/j.ijpx.2022.100116>.
26. Wang, J.; Li, Z.; Yin, Y.; Liu, H.; Tang, G.; Ma, Y.; Feng, X.; Mei, H.; Bi, J.; Wang, K. Mesoporous silica nanoparticles combined with MoS<sub>2</sub> and FITC for fluorescence imaging and photothermal therapy of cancer cells. *Journal of Materials Science* **2020**, *55*, 15263-15274, <https://doi.org/10.1007/s10853-020-04950-7>.
27. Jänicke, P.; Lennicke, C.; Meister, A.; Seliger, B.; Wessjohann, L.A.; Kaluderović, G.N. Fluorescent spherical mesoporous silica nanoparticles loaded with emodin: synthesis, cellular uptake and anticancer activity. *Materials Science and Engineering: C* **2021**, *119*, 111619, <https://doi.org/10.1016/j.msec.2020.111619>.
28. Lei, Q.; Guo, J.; Noureddine, A.; Wang, A.; Wuttke, S.; Brinker, C.J.; Zhu, W. Sol-gel-based advanced porous silica materials for biomedical applications. *Advanced Functional Materials* **2020**, *30*, 1909539, <https://doi.org/10.1002/adfm.201909539>.
29. Fu, Z.; Li, L.; Wang, Y.; Chen, Q.; Zhao, F.; Dai, L.; Chen, Z.; Liu, D.; Guo, X. Direct preparation of drug-loaded mesoporous silica nanoparticles by sequential flash nanoprecipitation. *Chemical Engineering Journal* **2020**, *382*, 122905, <https://doi.org/10.1016/j.cej.2019.122905>.
30. Kankala, R.K.; Han, Y.H.; Na, J.; Lee, C.H.; Sun, Z.; Wang, S.B.; Kimura, T.; Ok, Y.S.; Yamauchi, Y.; Chen, A.Z. Nanoarchitected structure and surface biofunctionality of mesoporous silica nanoparticles. *Advanced materials* **2020**, *32*, 1907035, <https://doi.org/10.1002/adma.201907035>.
31. Alfheid, L.H.K. Adsorption of paracetamol in contaminated water through pH-responsive polymer-brush-grafted mesoporous silica nanoparticles. *International Journal of Environmental Analytical Chemistry* **2024**, *104*, 776-792, <https://doi.org/10.1080/03067319.2022.2025789>.
32. Moghaddam, S.P.H.; Mohammadpour, R.; Ghandehari, H. In vitro and in vivo evaluation of degradation, toxicity, biodistribution, and clearance of silica nanoparticles as a function of size, porosity, density, and composition. *Journal of controlled release: Official journal of the Controlled Release Society* **2019**, *311-312*, 1-15, <https://doi.org/10.1016/j.jconrel.2019.08.028>.
33. Tao, Y.; Xu, S.; Wang, J.; Xu, L.; Zhang, C.; Chen, K.; Lian, Z.; Zhou, J.; Xie, H.; Zheng, S. Delivery of microRNA-33 antagomirs by mesoporous silica nanoparticles to ameliorate lipid metabolic disorders. *Frontiers in Pharmacology* **2020**, *11*, 921, <https://doi.org/10.3389/fphar.2020.00921>.
34. Rizzi, F.; Castaldo, R.; Latronico, T.; Lasala, P.; Gentile, G.; Lavorgna, M.; Striccoli, M.; Agostiano, A.; Comparelli, R.; Depalo, N. High surface area mesoporous silica nanoparticles with tunable size in the sub-micrometer regime: insights on the size and porosity control mechanisms. *Molecules* **2021**, *26*, 4247, <https://doi.org/10.3390/molecules26144247>.
35. Abbaszadegan, A.; Ghahramani, Y.; Gholami, A.; Hemmateenejad, B.; Dorostkar, S.; Nabavizadeh, M.; Sharghi, H. The effect of charge at the surface of silver nanoparticles on antimicrobial activity against gram-positive and gram-negative bacteria: a preliminary study. *Journal of Nanomaterials* **2015**, *16*, 53-53, <https://doi.org/10.1155/2015/720654>.

36. Rodrigues, G.R.; López-Abarrategui, C.; de la Serna Gómez, I.; Dias, S.C.; Otero-González, A.J.; Franco, O.L. Antimicrobial magnetic nanoparticles based-therapies for controlling infectious diseases. *International journal of pharmaceutics* **2019**, *555*, 356-367, <https://doi.org/10.1016/j.ijpharm.2018.11.043>.
37. Osman, N.; Devnarain, N.; Omolo, C.A.; Fasiku, V.; Jaglal, Y.; Govender, T. Surface modification of nano-drug delivery systems for enhancing antibiotic delivery and activity. *Nanomedicine and Nanobiotechnology* **2022**, *14*, e1758, <https://doi.org/10.1002/wnan.1758>.
38. Chen, X.; Liu, Y.; Lin, A.; Huang, N.; Long, L.; Gang, Y.; Liu, J. Folic acid-modified mesoporous silica nanoparticles with pH-responsiveness loaded with Amp for an enhanced effect against anti-drug-resistant bacteria by overcoming efflux pump systems. *Biomaterials science* **2018**, *6*, 1923-1935, <https://doi.org/10.1039/C8BM00262B>.